# Narrow escape through a funnel and effective diffusion on a crowded membrane

D. Holcman,[1,2] N. Hoze,[1] and Z. Schuss[2]
[1]*Ecole Normale Supérieure, Département de Mathématiques et de Biologie, 46 rue d'Ulm 75005 Paris, France*
[2]*Department of Applied Mathematics, Tel Aviv University, Tel Aviv 69978, Israel*
(Received 11 April 2011; revised manuscript received 19 June 2011; published 5 August 2011)

Particles diffusing on a membrane crowded with obstacles have to squeeze between them through funnel-shaped narrow straits. The computation of the mean passage time through the straits is a new narrow escape problem that gives rise to new, hitherto unknown, behavior that we communicate here. The motion through the straits on the coarse scale of the narrow escape time is an effective diffusion with coefficient that varies nonlinearly with the density of obstacles. We calculate the coarse-grained diffusion coefficient on a planar lattice of circular obstacles and use it to estimate the density of obstacles on a neuronal membrane and in a model of a cytoplasm crowded by identical parallel circular rods.

DOI: 10.1103/PhysRevE.84.021906 PACS number(s): 87.16.ad, 87.15.Vv, 02.50.Fz, 05.40.Jc

## I. INTRODUCTION

We consider free Brownian motion in a planar domain crowded with obstacles, which can be viewed as a simplified model of tracer motion on a neuronal membrane. Our purpose is to determine the relation between the variation in the obstacle density and in the effective diffusion coefficient in the high-crowding limit and to examine the quality of the asymptotic approximation by Brownian dynamics simulations. In our simplified model the obstacles are arranged in a square lattice of identical circles so at high crowding the separations between the obstacles become funnel-shaped narrow straits. The effective diffusion coefficient is inversely proportional to the mean passage time through the straits, which is the narrow escape time (NET). The computation of the mean passage time through the straits is a variant of the NET problem, previously considered in Refs. [1–8]. The new element in this computation is the geometry of the funnel-shaped narrow straits. This geometrical feature changes the dependence of the NET on the size of the opening relative to all cases considered previously. A numerical study of related problems was undertaken in Ref. [9] for the same planar geometry. As the straits become narrower the time scale of effective diffusion grows indefinitely and the numerical exploration of the parameter space becomes harder. A similar effect was observed in Ref. [10], where a numerical study of three-dimensional Brownian particles of finite size that have to squeeze through narrow openings between obstacles. An attempt at the analytical derivation of the effective diffusion coefficient in an array of spheres was considered in Ref. [11], where the NET through a circular window was used instead of the NET through a funnel. This article presents a new analytical expression for the effective diffusion coefficient and reveals an unexpected power-law decay as crowding increases. This purely geometrical effect is generic, because it is determined only by the immediate neighborhood of the narrow straits.

We apply this result to the calculation of the effective diffusion coefficient as a function of the obstacle density on the neuronal membrane. A reverse application can reconstruct the density of obstacles from the measured effective diffusion coefficient.

## II. FORMULATION AND MAIN RESULTS

The random motion of receptors on the surface of a neuron is usually restricted by many impenetrable obstacles. These often consist of noninteracting molecules, or fences, that are assemblies of several molecules, or corrals, that are collections of fences with small holes; microtubules and the cytoskeleton network can also form obstacles. The effect of obstacles on the diffusion coefficient has been studied in the biological context for the past two decades [12–19] and more recently it was demonstrated, using single-particle imaging [20–23], that the effective diffusion coefficient can span a large spectrum of values from 0.001 to 0.2 $\mu m^2/s$ [23].

We consider, for definiteness, a Brownian particle with diffusion coefficient $D$ in a planar domain $\Omega$ with a narrow neck [Fig. 1(a)] such that the opening for the passage of the particle is much smaller than the radius of curvature at the narrow neck and of the radius of the confining domain between the obstacles. The local geometry of the narrow passage can be described as the opening created from a cusp formed by two tangent circles that are moved slightly apart. The boundary of the domain $\Omega$, away from the cusp, whose diameter is assumed to be much larger than the width $\varepsilon = \overline{AB}$ of the neck, can be assumed, without loss of generality as shown below, to be enclosed by an arc of a circle of radius $R = O(1) \gg \varepsilon$ and two circular arcs of radius 1 in dimensionless units [Fig. 1(a)]. Our purpose is to calculate the mean first passage time (MFPT) from any point in $\Omega$, away from the immediate neighborhood of the funnel, to the segment AB.

The first new result of this paper is a new asymptotic approximation of the MFPT, given by

$$\bar{\tau} = \frac{\pi |\Omega|}{D\sqrt{\varepsilon}}[1 + O(\sqrt{\varepsilon})] \quad \text{for } \varepsilon \ll 1.$$

The second result is the uniform expansion (13) of the NET from one lattice square with reflecting circles centered at the corners.

## III. NET IN A CUSPED NARROW NECK

Our aim is to construct a leading-order asymptotic approximation in the limit $\varepsilon \ll 1$ to the MFPT $\bar{\tau}(x,y) = \mathbb{E}[\tau \mid (x(0),y(0)) = (x,y)]$ of a Brownian trajectory $(x(t),y(t))$

 

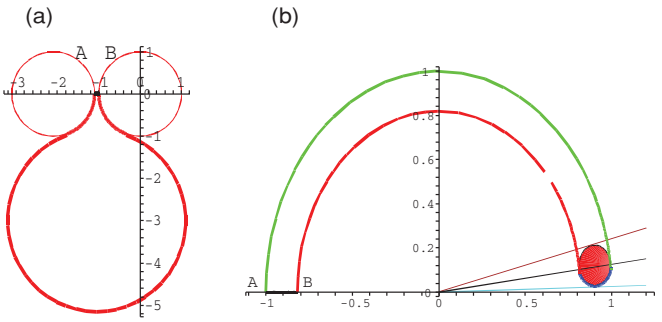


FIG. 1. (Color online) (a) Narrow straits formed by a cusp between two reflecting circles. The domain delimited by the big reflecting circle and the cusped neck is $\Omega$. A Brownian particle can escape $\Omega$ only through the segment AB. (b) The image $\Omega_w = w(\Omega)$ under the conformal mapping (2). The narrow neck leading to AB in $\Omega$ is mapped into the semi-ring-shaped domain in $\Omega_w$. The remaining part of $\Omega$ is mapped into the red domain. The segment AB (of length $\varepsilon$) in the left panel is mapped into the thick black segment AB in the right panel [of length $\sqrt{\varepsilon} + O(\varepsilon)$].

from points $(x,y) \in \Omega$, outside the immediate neighborhood of the narrow neck, to the segment $\mathrm{AB} = \partial\Omega_a$ [Fig. 1(a)]. We assume that the diffusion coefficient is $D$. The function $u(x,y) = \bar{\tau}(x,y)$ is the solution of the boundary value problem [24]

$$\begin{aligned} D\Delta u(x,y) &= -1 \quad \text{for } (x,y) \in \Omega, \\ \frac{\partial u(x,y)}{\partial n} &= 0 \quad \text{for } (x,y) \in \partial\Omega - \partial\Omega_a, \\ u(x,y) &= 0 \quad \text{for } (x,y) \in \partial\Omega_a. \end{aligned} \tag{1}$$

We put the origin of the complex plane $z = x + iy$ in the center of the right upper circle and map the domain $\Omega$ in Fig. 1(a) conformally by setting

$$w(z) = \frac{z - \alpha}{1 - \alpha z}, \tag{2}$$

where $\alpha = -1 \pm \sqrt{\varepsilon} + O(\varepsilon)$. The image of $\Omega$ in the $w$ plane is the domain $\Omega_w = w(\Omega)$ in Fig. 1(b). The straits in Fig. 1(a) are mapped onto the semiring enclosed between the red circular arcs and the large disk is mapped onto the small red disk. The radius of the small red disk and the elevation of its center above the real axis are $O(\sqrt{\varepsilon})$. The segment AB (of length $\varepsilon$) is mapped onto the thick black segment **AB** in the $w$ plane [of length $\sqrt{\varepsilon} + O(\varepsilon)$].

Setting $u(z) = v(w)$, system (1) is converted to

$$\begin{aligned} \Delta_w v(w) &= -\frac{1}{D|w'(z)|^2} \\ &= -\frac{4\varepsilon + O(\varepsilon)^{3/2}}{D|w(1-\sqrt{\varepsilon}) - 1 + O(w\varepsilon)|^4} \quad \text{for } w \in \Omega_w, \end{aligned} \tag{3}$$

$$\begin{aligned} \frac{\partial v(w)}{\partial n} &= 0 \quad \text{for } w \in \partial\Omega_w - \partial\Omega_{w,a}, \\ v(w) &= 0 \quad \text{for } w \in \partial\Omega_{w,a}. \end{aligned} \tag{4}$$

The MFPT from $\Omega$ to the segment AB equals that from the inverse image of a ring at an intermediate angle $\theta = c\sqrt{\varepsilon}$ (black line around the circle). The solution of the boundary value problem [Eqs. (3) and (4)] is to leading order independent of the radial variable in polar coordinates $w = re^{i\theta}$. Fixing $r = 1$, we impose the reflecting boundary condition at $\theta = c\sqrt{\varepsilon}$, where $c = O(1)$ is a constant independent of $\varepsilon$ to leading order and the absorbing condition at $\theta = \pi$. Thus, we obtain the leading-order approximation

$$v(e^{i\theta}) = \frac{4\varepsilon}{D}\int_{\theta}^{\pi} \frac{(\pi - \eta)\,d\eta}{|e^{i\eta} - 1 - e^{i\eta}\sqrt{\varepsilon}|^4}[1 + O(\sqrt{\varepsilon})]. \tag{5}$$

After evaluating asymptotically each integral, we get

$$v(e^{ic\sqrt{\varepsilon}}) = \frac{4\pi C}{D\sqrt{\varepsilon}}[1 + O(\sqrt{\varepsilon})], \tag{6}$$

where $C = O(1)$ is a constant. To determine the value of the constant $C$, we use the flux condition and compute the derivative

$$\begin{aligned} \left.\frac{\partial v(e^{i\theta})}{\partial n}\right|_{\partial\Omega_{w,a}} &= \left.\frac{\partial v}{\partial\theta}\right|_{\theta=\pi} = -\frac{4\varepsilon}{D}\int_{c\sqrt{\varepsilon}}^{\pi} \frac{d\eta}{|e^{i\eta} - 1 - e^{i\eta}\sqrt{\varepsilon}|^4} \\ &= -\frac{4C}{D\sqrt{\varepsilon}}[1 + O(\sqrt{\varepsilon})] \end{aligned} \tag{7}$$

and integration of (1) over $\Omega_w$ gives

$$\sqrt{\varepsilon}\left.\frac{\partial v(e^{i\theta})}{\partial n}\right|_{\partial\Omega_{w,a}} = -\frac{|\Omega|}{D}. \tag{8}$$

Now (7) and (8) imply that $4C = |\Omega|$ so the NET $\bar{\tau}$ to AB from $(x,y) \in \Omega$, outside the straits, is to leading order independent of $(x,y)$ and is given by

$$\bar{\tau} = \frac{\pi|\Omega|}{D\sqrt{\varepsilon}}(1 + O(\sqrt{\varepsilon})) \quad \text{for } \varepsilon \ll |\partial\Omega|. \tag{9}$$

The graphs of the solution $v(e^{i\theta})$ of (4) for $\varepsilon = 10^{-1}, 10^{-2}, 10^{-3}$ and of $\bar{\tau}$ versus $\varepsilon$ are given in Fig. 2. The boundary layer, which stretches up to about $\theta = 1.5$, is the inverse image of this part of the ring and occupies small part of the straits leading to the absorbing boundary at AB. In

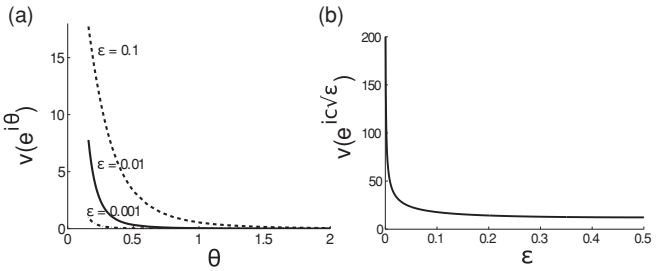


FIG. 2. (a) The solution $v(e^{i\theta})$ for $\varepsilon = 10^{-1}, 10^{-2}, 10^{-3}$. (b) The NET $v(e^{ic\sqrt{\epsilon}})$ for $c = 0.5$.

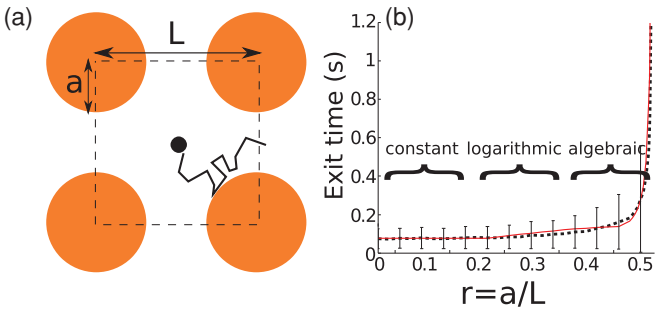


FIG. 3. (Color online) NET from the domain (a) with $D = 1$, $L = 1$. Statistics were obtained from 1000 exit times of simulated Brownian trajectories (dashed line). (b) NET vs. obstacle scaled radius $r = a/L = \frac{1}{2}(1-\varepsilon)$. The analytical approximation is [Eq. (13), continuous curve] with $0 < r = r_1 = 0.2$, $r_1 < r < r_2 = 0.45$, and $0.45 < r < 0.5$.

dimensional variables, the NET (9) is given by

$$\bar{\tau} = \frac{\pi|\Omega|}{D\sqrt{\varepsilon/R}}\left[1 + O\left(\sqrt{\frac{\varepsilon}{R}}\right)\right], \tag{10}$$

where $R$ is the radius of curvature at the cusp.

## IV. NET FROM A LATTICE SQUARE BOUNDED BY OBSTACLES

Next, we consider the NET from a square of side $L$ with reflecting circles of radius $a$ centered at the corners [Fig. 3(a)] over the entire range of possible straits. First, we note that if there are $n$ well-separated identical escape routes through narrow straits, then, according to Refs. [7,25], the NET is independent of $(x,y)$ to leading order and can be approximated by

$$\bar{\tau}_n = \frac{\bar{\tau}}{n}, \tag{11}$$

where $\bar{\tau}$ is the MFPT to a single escape window in a neck with the other windows closed (reflecting instead of absorbing).

For small $a \ll L$, the NET is independent of $a$, though dependent on $(x,y)$, so the circles can be ignored to leading order [Eq. (14)], but it increases with $a$. When the width of the straits $L - 2a$ is about $2a$, that is, when $a \approx L/4$, the opening between the circles can be considered small, so according to Refs. [7,25] and (11) it can be approximated by

$$\bar{\tau} = \frac{|\Omega|}{4D\pi}\left[\log\frac{1}{\varepsilon} + O(1)\right] \quad \text{with} \quad \varepsilon = (L-2a)/L \approx 0.5, \tag{12}$$

because there are four well-separated straits for escape. For $L - 2a \ll a/2$ (i.e., for $\varepsilon \ll 1$), the analysis of the previous paragraph applies and we have (11). Thus a uniform approximation to the NET from the center can be obtained by patching the three regimes numerically, which gives

$$\bar{\tau} \approx \begin{cases} c_1 & \text{for } 0.8 < \varepsilon < 1, \\ c_2|\Omega|\log\frac{1}{\varepsilon} + d_1 & \text{for } 0.55 < \varepsilon < 0.8, \\ c_3\frac{|\Omega|}{\sqrt{\varepsilon}} + d_2 & \text{for } \varepsilon < 0.55, \end{cases} \tag{13}$$

with $d_1, d_2 = O(1)$. The MFPT $c_1$ from the center to the boundary of an unrestricted square is the value of the solution of (1), given by

$$u(x,y) = \frac{4L^2}{\pi^3 D}\sum_0^\infty \frac{\left[\cosh\left(k+\frac{1}{2}\right)\pi - \cosh\left(k+\frac{1}{2}\right)\pi(2y/L-1)\right]\sin(2k+1)\pi x/L}{(2k+1)^3\cosh(2k+1)\pi}, \tag{14}$$

so $c_1 = u(L/2, L/2) \approx [4L^2/\pi^3 D][\cosh(\pi/2-1)/\cosh\pi]$. For $L = 1, D = 1$, we find $c_1 \approx 0.076$, in agreement with Brownian dynamics simulations [Fig. 3(b)]. The coefficient $c_2$ is obtained from (12) as $c_2 = 1/2\pi D \approx 0.16$. Similarly, the coefficient $c_3$ is obtained from (10), (11) as $c_3 \approx \pi/4\sqrt{2}\,D \approx 0.56$. The coefficients $d_i$ are chosen by patching $\bar{\tau}$ continuously between the different regimes. We get

$$d_1 = c_1 + c_2|\Omega(r_1)|\log(1-2r_1) \tag{15}$$

and

$$d_2 = c_1 - c_2[|\Omega(r_1)|\log(1-2r_1) + |\Omega(r_2)|\log(1-2r_2)] - c_3|\Omega(r_2)|(1-2r_2)^{-1/2}.$$

Simulations with $D = 1$ in a square of radius $L = 1$ with four reflecting circles of radius $r$, centered at the corners, show that the uniform approximation by the patched formula (13) is in good agreement with Brownian results [Fig. 3(b)], where the statistics were collected from 1000 escape times of Brownian trajectories per graph point. The trajectories start at the square center.

## V. DIFFUSION OF RECEPTORS ON THE NEURONAL MEMBRANE

To calculate the effective diffusion coefficient of the Brownian motion on an isotropic square lattice with crowded obstacles in a domain $\Omega$ with a reflecting boundary, we first coarse-grain it into a random walk between the centers of adjacent squares. Then we approximate the master equation for the transition probability density function of the random walk by the two-dimensional diffusion equation [26]. Because the mean exit time from a single lattice square is long, the first eigenvalue of the mixed Dirichlet-Neumann problem in a single cell is well separated from the higher ones. It follows that the waiting time in the cell is exponentially distributed [24] with rate

$$\lambda = \frac{1}{2\bar{\tau}}, \tag{16}$$

where $\bar{\tau}$ is given in Eq. (13). This is due to the fact that a Brownian trajectory at the center of the straits is equally likely to return or move to the next lattice square, much like in atomic migration in crystals [26]. The diffusion approximation to the

master equation for the transition probability density function of an isotropic random walk that jumps at exponentially distributed waiting times with rate $\lambda$ on a square lattice with step size $L$ is given by [26]

$$\frac{\partial p}{\partial t} = \bar{D}\left(\frac{\partial^2 p}{\partial x^2} + \frac{\partial^2 p}{\partial y^2}\right), \quad \bar{D} = \frac{\lambda L^2}{4}. \tag{17}$$

Next, we apply the above results to the estimation of the density of obstacles on the membrane of a neuronal dendrite. Using the experimentally measured single receptor trajectory on the surface of a neuron by single-particle tracking methods, we use that the receptor effective diffusion coefficient varies from 0.01 to 0.2 $\mu$m$^2$/s [20,22,23]. In our simplified model of crowding, the circular obstacles are as in Fig. 4(a). We simulated Brownian trajectories and recorded the escape NET from one square to the other [Fig. 4(a)] with fixed $L$ and variable $a$. According to Eqs. (13), (16), and (17), as $a$ increases the effective diffusion coefficient $\bar{D}$ decreases. Using the mean-square displacement (MSD), we computed the effective diffusion coefficient $\langle \frac{\mathrm{MSD}(t)}{4t} \rangle$ [Fig. 2(b)] from our Brownian simulations and found that it is linear, thus confirming that in such geometry, crowding does not affect the nature of the Brownian motion for sufficiently large time (for a diffusion coefficient of $D = 0.2$ $\mu$m$^2$/s, we are considering a time larger than 10 s). In addition, Fig. 4(c) shows the diffusion coefficient ratio $D_a/D_0$, where $D_a$ was computed from the MSD of the Brownian simulations on the square lattice described above with obstacles of radius $a$. For $a = 0.3$, we find that $D_a/D_0 \approx 0.7$, whereas a direct computation using of the mean exit time formula (13) gives

$$\tau_0/\tau_a = \frac{c_1}{c_2|\Omega| \log \frac{1}{\varepsilon} + d_1} \approx 0.69, \tag{18}$$

where $\varepsilon = \frac{L-2a}{L} = 0.4$. We conclude from our simulations that the coarse-grained diffusion is classical and the effective diffusion coefficient $D_a/D_0 = \tau_0/\tau_a$ decreases nonlinearly as a function of the radius $a$, as given by the uniform formula (13). We recover the three regimes of Eq. (13) [Fig. 4(c)]: a noncrowded regime for $a < 0.2L$, where the effective diffusion coefficient does not show any significant decrease, a region $0.2L < a < 0.4L$, where the leading order term of the effective diffusion coefficient is logarithmic, and for $a > 0.4L$ the effective diffusion coefficient decays as $\sqrt{(L-2a)/L}$, in agreement with Eq. (13).

Finally, to estimate the density of obstacles in a neuron from Eqs. (13), (16), and (17), a reference density has to be chosen. We choose that the reference diffusion coefficient of AMPA receptors moving on a free membrane (with removed cholesterol), estimated to be $0.17 \leqslant D \leqslant 0.2$ $\mu$m$^2$/s [27], while with removing actin, is 0.19 $\mu$m$^2$/s. We used this $D = 0.2$ $\mu$m$^2$/s to estimate the crowding effect based on the measured diffusion coefficient [Fig. 2(d)]: We found that a reduction of the diffusion coefficient from $D = 0.2$ $\mu$m$^2$/s to $D = 0.04$ $\mu$m$^2$/s is achieved when 70% of the membrane surface is occupied by obstacles. We conclude that obstacles impair the diffusion of receptors and are thus responsible for the large decrease of the measured diffusion coefficient (up to 5 times).

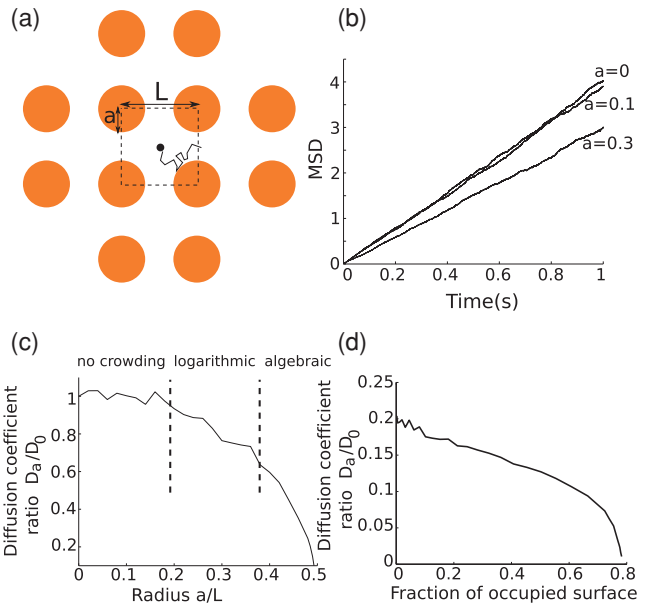


FIG. 4. (Color online) Organization of the neuronal membrane. (a) Schematic representation of a Brownian particle diffusing in a crowded microdomain. (b) Mean-square displacement (MSD) of the particle in a domain paved with microdomains. The MSD is linear, showing that crowding does not affect the nature of diffusion. The effective diffusion coefficient is computed from $\langle \mathrm{MSD}(t)/4t \rangle$ ($D = 1$). (c) Effective diffusion coefficient computed from the MSD for different radiuses of the obstacles. Brownian simulations (continuous curve): there are three regions (separated by the dashed lines). While there is no crowding for $a < 0.2$, the decreasing of the effective diffusion coefficient for $0.2 < a < 0.4$ is logarithmic and like the square root for $a > 0.4$. (d) Effective diffusion coefficient of a particle diffusing in a domain as a function of the fraction of the occupied surface. An $\alpha$-amino-3-hydroxy-5-methyl-4-isoxazolepropionic acid (AMPAR) receptor has a diffusion coefficient of 0.2 $\mu$m$^2$/s in a free membrane [27].

## VI. SUMMARY

The local geometry of the exit route of a Brownian particle through a small portion of the boundary of a planar domain has profound influence on the mean escape time. We have found here that the NET through a funnel, a problem hitherto unsolved, increases as the power law $\varepsilon^{-1/2}$ that was not observed in any of the planar geometries studied so far. This indicates that the singularity of Green's function for the mixed Neumann-Dirichlet boundary value problem for the Laplace equation depends strongly on the narrow opening on the geometric properties of the boundary there. A similar behavior is observed in three dimensions as well.

The application of the new law to the coarse-graining of Brownian motion in a domain crowded by a lattice of circular obstacles, first, by a random walk on the lattice and then by an effective diffusion, shows that the effective diffusion coefficient varies nonlinearly with obstacle density. A small increase in the concentration of obstacles at very large crowding leads to a sharp decrease of the effective diffusion coefficient. We note that the coarse-graining is valid on a time scale much longer than the NET, so no anomalous effects are observed on this scale. The present approach can

be applied to the three-dimensional cytoplasm crowded by parallel cylindrical obstacles. The case of other geometries is yet to be done.

The present study of coarse-grained diffusion arises in a model of receptor diffusion on a synaptic membrane of a neuron. The route of a receptor inserted into the membrane to its destination in the postsynaptic density (PSD) is obstructed with many impenetrable structures. A biological interpretation of our results may be that the large change in arrival time, and thus in the population of the PSD, may indicate a possible mechanism of permanent physiological modulation by adding a small number of obstacles to the crowded membrane.

## ACKNOWLEDGMENT

This research is supported by an ERC starting grant.

[1] A. Singer and Z. Schuss, Phys. Rev. E **74**, 020103(R) (2006).
[2] Z. Schuss, A. Singer, and D. Holcman, Proc. Natl. Acad. Sci. USA **104**, 16098 (2007).
[3] M. J. Ward and J. B. Keller, SIAM J Appl. Math. **53**, 770 (1993).
[4] M. J. Ward, W. D. Henshaw, and J. B. Keller, SIAM J Appl. Math. **53**, 799 (1993).
[5] M. J. Ward and E. Van De Velde, IMA J. Appl. Math. **48**, 53 (1992).
[6] T. Kolokolnikov, M. Titcombe, and M. J. Ward, European J. Appl. Math. **16**, 161 (2005).
[7] D. Holcman and Z. Schuss, J. Stat. Phys. **117**, 191 (2004).
[8] A. Singer, Z. Schuss, and D. Holcman, J. Stat. Phys. **122**, 491 (2006).
[9] H. X. Zhou and R. Zwanzig, J. Chem. Phys. **94**, 6147 (1991).
[10] P. A. Netz and T. Dorfmüller, J. Chem. Phys. **107**, 9221 (1997).
[11] A. M. Berezhkovskii, V. Yu. Zitserman, and S. Y. Shvartsman, J. Chem. Phys. **118**, 7146 (2003).
[12] M. Edidin, S. C. Kuo, and M. P. Sheetz, Science **254**, 1379 (1991).
[13] M. P. Sheetz, Annu. Rev. Biophys. Biomol. Struct. **22**, 417 (1993).
[14] K. Suzuki and M. P. Sheetz, Biophys. J. **81**, 2181 (2001).
[15] A. Kusumi *et al*., Annu. Rev. Biophys. Biomol. Struct. **34**, 351 (2005).
[16] A. Kusumi, Y. Sako, and M. Yamamoto, Biophys. J. **65**, 2021 (1993).
[17] M. J. Saxton, Biophys. J. **69**, 389 (1995).
[18] M. J. Saxton and K. Jacobson, Annu. Rev. Biophys. Biomol. Struct. **26**, 373 (1997).
[19] J. Eisinger, J. Flores, and W. P. Petersen, Biophys. J. **49**, 987 (1986).
[20] A. J. Borgdorff and D. Choquet, Nature **417**, 649 (2002).
[21] C. Tardin *et al*., EMBO J. **22**, 4656 (2003).
[22] D. Choquet and A. Triller, Nat. Rev. Neurosci. **4**, 251 (2003).
[23] D. Choquet, Eur. J. Neurosci. **32**, 250 (2010).
[24] Z. Schuss, *Theory and Applications of Stochastic Processes* (Springer, New York, 2010).
[25] D. Holcman and Z. Schuss, Phys. Lett. A **372**, 3768 (2008).
[26] Z. Schuss, *Theory and Applications of Stochastic Differential Equations* (Wiley, New York, 1980).
[27] M. Renner, D. Choquet, and A. Triller, J. Neurosci. **29**, 2926 (2009).